Accurate and efficient computation of nonlocal potentials based on Gaussian-sum approximation

Lukas Exl[a,b], Norbert J. Mauser[c], Yong Zhang[c,*]

[a]Fak. Mathematik, Univ. Wien, Oskar-Morgenstern-Platz 1, 1090, Vienna.
[b]Inst. of Solid State Physics, TU Wien, Karlsplatz 13, 1040, Vienna.
[c]Wolfgang Pauli Institute c/o Fak. Mathematik, Univ. Wien, Oskar-Morgenstern-Platz 1, 1090, Vienna.

Abstract

We introduce an accurate and efficient method for the numerical evaluation of nonlocal potentials, including the 3D/2D Coulomb, 2D Poisson and 3D dipole-dipole potentials. Our method is based on a Gaussian-sum approximation of the singular convolution kernel combined with a Taylor expansion of the density. Starting from the convolution formulation of the nonlocal potential, for smooth and fast decaying densities, we make a full use of the Fourier pseudospectral (plane wave) approximation of the density and a separable Gaussian-sum approximation of the kernel in an interval where the singularity (the origin) is excluded. The potential is separated into a regular integral and a near-field singular correction integral. The first is computed with the Fourier pseudospectral method, while the latter is well resolved utilizing a low-order Taylor expansion of the density. Both parts are accelerated by fast Fourier transforms (FFT). The method is accurate (14-16 digits), efficient ($O(N \log N)$ complexity), low in storage, easily adaptable to other different kernels, applicable for anisotropic densities and highly parallelizable.

Keywords: nonlocal potential solver, convolution integral, separable Gaussian-sum approximation, Coulomb/Poisson/dipole-dipole potential, singular correction integral

1. Introduction

Nonlocal potentials, like the Newtonian potential, occur in a variety of mathematical models in electrostatics, plasma, quantum physics/chemistry to material and life sciences etc. Efficient and accurate numerical calculation of such nonlocal potentials is an active and important topic in the science and engineering community. In this paper, we deal with nonlocal potentials, in a setting on the whole space $\mathbb{R}^d$, given originally by convolutions:

$$u(\mathbf{x}) = (U * \rho)(\mathbf{x}) = \int_{\mathbb{R}^d} U(\mathbf{x} - \mathbf{y})\rho(\mathbf{y})d\mathbf{y}, \qquad \mathbf{x} \in \mathbb{R}^d, \quad d = 2, 3, \tag{1.1}$$

where $*$ denotes the convolution operator, $\rho(\mathbf{x})$ is the density function, and $U(\mathbf{x})$ is a nonlocal (long-range) kernel. For instance, the 3D Coulomb potential with $U(\mathbf{x}) = \frac{1}{4\pi|\mathbf{x}|}$, is fundamental in many fields of physics including the Bose-Einstein Condensates [3, 4, 7, 33, 32], and quantum chemistry[18, 19, 20, 24].

In this paper, we study several important nonlocal potentials with their kernels given explicitly as

$$U(\mathbf{x}) = \begin{cases} \frac{1}{4\pi|\mathbf{x}|}, & 3D \text{ Coulomb}, \\ \frac{1}{2\pi|\mathbf{x}|}, & 2D \text{ Coulomb}, \\ -\frac{1}{2\pi} \ln|\mathbf{x}|, & 2D \text{ Poisson}. \end{cases} \tag{1.2}$$

---

*Corresponding author.
Email addresses: `lukas.exl@univie.ac.at` (Lukas Exl), `norbert.mauser@univie.ac.at` (Norbert J. Mauser), `yong.zhang@univie.ac.at` (Yong Zhang)

Also the dipole-dipole convolution kernel $U(\mathbf{x}) = \frac{3}{4\pi} \frac{\mathbf{m}\cdot\mathbf{n} - 3(\mathbf{x}\cdot\mathbf{n})(\mathbf{m}\cdot\mathbf{x})/|\mathbf{x}|^2}{|\mathbf{x}|^3}$, with $\mathbf{n}, \mathbf{m} \in \mathbb{R}^3$ unit vectors, can be reformulated through the above mentioned kernels [3, 4, 7, 23, 32, 33].

The density ρ is assumed to be smooth and fast decaying, as it is common in many applications. Therefore, in this paper, we can reasonably assume that the density is compactly supported (numerically) in a finite domain $\mathbf{B}$, more precisely,

$$\text{supp}_{\text{num}}(\rho) := \{\mathbf{x} \,\big|\, \text{s.t.} |\rho(\mathbf{x})| > 10^{-16}\} \subset \mathbf{B}.$$

In this situation, the (discrete) Fourier method is a good candidate to approximate the density. Yet, the convolution kernel and its Fourier transform are both singular at the origin and/or at the far-field, which requires special numerical effort.

In the past few years, different techniques have been proposed in the literature, such as the Fast Multipole Method (FMM) [14, 21], the Non-Uniform Fast Fourier Transform (NUFFT) [23, 6, 17] and Gaussian-Sum (GS) approximations [8, 19, 20, 16, 17], etc. In the following, we briefly mention some of them and discuss their advantages and disadvantages respectively.

The convolution (1.1) can be represented formally as a Fourier integral

$$u(\mathbf{x}) = \frac{1}{(2\pi)^d} \int_{\mathbb{R}^d} \widehat{U}(\mathbf{k})\widehat{\rho}(\mathbf{k}) \, e^{i\mathbf{k}\cdot\mathbf{x}} d\mathbf{k}, \qquad \mathbf{x} \in \mathbb{R}^d, \tag{1.3}$$

where $\widehat{f}(\mathbf{k}) = \int_{\mathbb{R}^d} f(\mathbf{x}) \, e^{-i\mathbf{k}\cdot\mathbf{x}} \, d\mathbf{x}$ is the Fourier transform of $f(\mathbf{x})$ for $\mathbf{x}, \mathbf{k} \in \mathbb{R}^d$. Note that the Fourier transform of the convolution kernel $\widehat{U}(\mathbf{k})$ is also long-range and singular, and sometimes the singularity is too strong that the Fourier representation is not well-defined, e.g., $1/|\mathbf{k}|^2$ for the 2D Poisson potential [6].

Another important equivalent formulation is to solve a partial differential equation (PDE) in whole space $\mathbb{R}^d$ with appropriate far-field decay condition. For instance, the 3D Coulomb potential satisfies the Poisson equation, i.e.,

$$-\Delta \, u(\mathbf{x}) = \rho(\mathbf{x}), \qquad \mathbf{x} \in \mathbb{R}^3, \qquad \lim_{|\mathbf{x}|\to\infty} u(\mathbf{x}) = 0. \tag{1.4}$$

All of the three formulations, (1.1), (1.3) and (1.4), are challenging numerically. In (1.1) and (1.3), the convolution kernels and their Fourier transforms are long-range and singular at the origin and/or at the far-field. Therefore, it requires either a large computation domain or elaborate strategies to take care of the singularity in physical and/or phase space. Various numerical methods have been proposed via the PDE approach on a rectangular domain with uniform mesh grid[4, 5, 34]. In the case of the 3D/2D Coulomb potential the following difficulties arise. As the potential decays to zero at the far-field, the commonly used periodic and homogeneous Dirichlet boundary conditions, imposed on the boundary of the rectangular domain, do not agree very well with the far-field asymptotics. Errors coming from the boundary condition approximation dominate as the mesh size tends smaller. The saturated accuracy achieved by Fourier/Sine pseudospectral methods, also referred to as "locking" accuracy, improves when the domain size increases [3, 4, 6, 7]. For the 2D Poisson potential, however, periodic or zero boundary conditions are inappropriate at all, because the potential diverges, i.e., $u(\mathbf{x}) \to C \ln|\mathbf{x}|, C > 0$ as $\mathbf{x} \to \infty$. Exact artificial boundary conditions on a disk were given by Zhang et al [25], while appropriate boundary conditions on the rectangular domain remain to be further explored.

Starting from the Fourier integral (1.3), a direct plane-wave discretization suffers serious accuracy loss due to improper treatment of the singularity in $\widehat{U}$ [6, 7, 18]. For kernels with removable singularity in spherical/polar coordinates, e.g., the 3D/2D Coulomb potential, Jiang, Greengard and Bao[23] proposed an accurate and efficient method which splits the kernel into a long-range regular and a short-range singular part, and evaluates the quadrature via Fast Fourier Transform (FFT) and nonuniform FFT (NUFFT) [13], respectively. This approach was recently adapted to the 2D Poisson case [6], whose singularity is too strong to be canceled out in polar coordinates. Their methods can achieve spectral accuracy with great efficiency that is inherited from the FFT and NUFFT algorithm. However, it is not ideal because of the large prefactor in front of the $O(N \log N)$ coming from the NUFFT [13, 23]. In addition, the 3D Coulomb/dipole-dipole evaluation is rather slow and it needs further investigation for practical simulations.

It is more natural to start from the convolution form (1.1), as it has been done in many approaches, see [8, 12, 18, 19, 20]. A basic idea is to modify the kernel somehow and to evaluate the long-range interaction efficiently. Several methods have been proposed, such as the Ewald-type partition[24, 18], the kernel-truncation [12], the Gaussian-sum (GS) approximation [8, 19, 20] etc. Among them, the Gaussian-sum based method is one of the most effective and accurate methods. The approximation of the kernel function by Gaussian/exponential sums has been studied intensively, we refer the reader to [9, 10, 11, 29]. In [8], Beylkin et al. split the 2D/3D Helmholtz potential into a convolution with Gaussian-sum in the spatial domain and a band-limited multiplier in the Fourier domain. Later, Genovese et al.[19] computed the Poisson potential by combining the interpolating scaling function (ISF) representation of the density and the Gaussian-sum approximation. However, the best achieved accuracy in [19], around 10-digits, is limited by the accuracy of the GS approximation. In fact, a near-field correction integral could have been incorporated into their method.

To sum up, the NUFFT approach introduces an accurate quadrature to evaluate the correction integral, while the advantage of the GS approximation, used in the ISF approach, is mostly due to its separable structure. Our new method aim to combine both advantages. To this end, we adopt the Gaussian-sum approximation for the long-range regular integral and compute the near-field correction integral with a local interpolation (a low-order Taylor expansion) instead of the global spectral interpolation (e.g., the NUFFT in [23]).

In our method, we represent the convolution kernel smoothly via a sum of Gaussian functions. Since this approximation is not accurate near the origin, a correction is applied to address the discrepancies between the Gaussian-sum and the original kernel function. Thus, we split the convolution (1.1) into two parts

$$u(\mathbf{x}) = \int_{\mathbb{R}^d} U_{GS}(\mathbf{y}) \, \rho(\mathbf{x} - \mathbf{y}) d\mathbf{y} + \int_{\mathbb{R}^d} \left(U(\mathbf{y}) - U_{GS}(\mathbf{y}) \right) \rho(\mathbf{x} - \mathbf{y}) d\mathbf{y}, \qquad (1.5)$$

where U_{GS} is the *Gaussian sum* (GS) approximation. The first integral in (1.5) is regular and computed by finite Fourier series method. The second integral contains a singular kernel, whose effective support is a small neighborhood of the origin. As a consequence, the second integral is essentially a local correction.

For the sake of simplicity, we choose a square box $\mathbf{B}_L := [-L, L]^d \subset \mathbb{R}^d, d = 2, 3$ (a general rectangular box is also feasible), and $\mathbf{B}_L$ is also domain of interest. Following a standard scaling argument, we first rescale the density to be compactly supported in the unit box $\mathbf{B}_1$, i.e.,

$$\mathbf{x} = \widetilde{\mathbf{x}} \, L, \quad \rho(\mathbf{x}) = \widetilde{\rho}(\widetilde{\mathbf{x}}), \quad \Longrightarrow \quad \widetilde{\mathbf{x}} \in \mathbf{B}_1, \ \text{supp}(\widetilde{\rho}) \subset \mathbf{B}_1. \qquad (1.6)$$

Plugging (1.6) into the convolution (1.1), we have

$$u(\mathbf{x}) = \int_{\mathbb{R}^d} U(\mathbf{x} - \mathbf{y})\rho(\mathbf{y})d\mathbf{y} = \int_{\mathbf{B}_L} U(\mathbf{x} - \mathbf{y})\rho(\mathbf{y})d\mathbf{y} = L^d \int_{\mathbf{B}_1} \widetilde{U}(\widetilde{\mathbf{x}} - \widetilde{\mathbf{y}})\widetilde{\rho}(\widetilde{\mathbf{y}})d\widetilde{\mathbf{y}}.$$

Particularly, for the 2D/3D Coulomb potentials, we have $\widetilde{U}(\widetilde{\mathbf{x}}) = U(\mathbf{x}) = U(\widetilde{\mathbf{x}}L) = L^{-1}U(\widetilde{\mathbf{x}})$, therefore,

$$u(\mathbf{x}) = \widetilde{u}(\widetilde{\mathbf{x}}) = L^{d-1} \int_{\mathbf{B}_1} U(\widetilde{\mathbf{x}} - \widetilde{\mathbf{y}})\widetilde{\rho}(\widetilde{\mathbf{y}})d\widetilde{\mathbf{y}}, \qquad \widetilde{\mathbf{x}} \in \mathbf{B}_1, \quad d = 2, 3.$$

Similarly, for the 2D Poisson potential, we have

$$u(\mathbf{x}) = \widetilde{u}(\widetilde{\mathbf{x}}) = -\frac{L^2}{2\pi} \int_{\mathbf{B}_1} \widetilde{\rho}(\widetilde{\mathbf{y}}) \ln |\widetilde{\mathbf{x}} - \widetilde{\mathbf{y}}| \, d\widetilde{\mathbf{y}} - \frac{L^2}{2\pi} \ln L \int_{\mathbf{B}_1} \widetilde{\rho}(\widetilde{\mathbf{y}}) \, d\widetilde{\mathbf{y}}, \quad \widetilde{\mathbf{x}} \in \mathbf{B}_1.$$

The domain of interest is also rescaled to $\mathbf{B}_1$. Therefore, the evaluation of $u(\mathbf{x})$ on $\mathbf{B}_L$ is equivalent to computing $\widetilde{u}(\widetilde{\mathbf{x}})$ on the unit box with rescaled density $\widetilde{\rho}(\widetilde{\mathbf{x}})$, which is also compactly supported in $\mathbf{B}_1$. We

3

shall omit ~ hereafter for simplicity. In practice, the computational domain $\mathbf{B}_1$ is usually discretized uniformly in each direction, and the density is given on the uniform grid $\mathcal{T}_h$:

$$\mathcal{T}_h = \{(x_{j_1}^{(1)}, \ldots, x_{j_d}^{(d)}) \big| x_{j_p}^{(p)} = -1 + j_p h^{(p)}, h^{(p)} = 2/n_p, 1 \le j_p \le n_p, p = 1, \ldots, d\}.$$

One of the key ideas of our method is to utilize a (separable) GS approximation of the convolution kernel so as to reformulate the potential into two integrals, namely, the *long-range regular integral* and the *short-range singular integral*. To be precise, we reformulate the potential (1.1) as follows:

$$u(\mathbf{x}) = \int_{\mathbb{R}^d} U_{GS}(\mathbf{y}) \, \rho(\mathbf{x} - \mathbf{y}) d\mathbf{y} + \int_{\mathbb{R}^d} \big(U(\mathbf{y}) - U_{GS}(\mathbf{y}) \big) \, \rho(\mathbf{x} - \mathbf{y}) d\mathbf{y} \tag{1.7}$$

$$:= I_1(\mathbf{x}) + I_2(\mathbf{x}), \qquad \mathbf{x} \in \mathbf{B}_1, \tag{1.8}$$

where U_{GS}, the GS approximation of the kernel, is given explicitly as follows:

$$U_{GS}(\mathbf{y}) = U_{GS}(|\mathbf{y}|) := \sum_{q=0}^{S} w_q \, e^{-\tau_q^2 |\mathbf{y}|^2}, \quad S \in \mathbb{N}^+, \tag{1.9}$$

with weights and nodes $\{(w_q, \tau_q)\}_{q=0}^S$. $I_1(\mathbf{x})$ is the long-range regular integral and the correction $I_2(\mathbf{x})$ is the short-range singular integral. It is noteworthy to point out that the singularity of the integrand of I_2 at the origin in physical space is canceled out in spherical/polar coordinates by the Jacobian of the coordinate transform.

The GS approximation is done over an interval excluding the origin, and computed numerically with *sinc quadrature* for an integral representation of the kernel function. The accuracy over an interval $[\delta, 2]$ is about $10^{-14} - 10^{-16}$ in relative/absolute L^∞-norm, whereas the parameter δ does not have to be as small as in [19]. In practice, we choose some intermediate values, e.g. $10^{-4}, 10^{-3}$. Therefore the effective support of the correction $U - U_{GS}$ is a δ-neighbourhood of the origin. The idea of exploiting the locality of the correction term resulting from a GS approximation has already been proven effective by Exl and Schrefl [17] in computational micromagnetics. This gives us the possibility to approximate the density with a local interpolation (Taylor expansion) in I_2.

The tensor product structure of the GS approximation is exploited for accurate and stable pre-computation of relevant coefficients, which are originally higher-dimensional integrals. The sinc quadrature approach gives us a suitable, fast and easily adaptable way to obtain the GS approximation, however, we shall remark that the sinc quadrature does not lead to an optimal approximation in terms of a minimal number of Gaussian terms. We refer to [11, 12, 17, 22] for more details.

The paper is organized as follows. In Section 2, we describe the algorithm, which consists of two steps: long-range regular integral evaluation, short-range singular integral evaluation. Then we present extensions to dipole-dipole potentials. A detailed error analysis is given, too. In Section 3, we present details on the Gaussian-sum approximation of two kernels, i.e., the Coulomb kernel $1/r$ and 2D Poisson kernel $\ln r$, by sinc quadrature. In Section 4, extensive numerical results are given to illustrate the performance of our new method in both accuracy and efficiency. Finally, some concluding remarks are drawn in Section 5.

2. Numerical algorithm

Following the previous discussion, we shall illustrate the computation of I_1 and I_2, present a detailed analysis in terms of accuracy and efficiency, and discussion possible extensions to some important models.

2.1. Evaluation of the regular integral $I_1(\mathbf{x})$

Due to the compact support of the density, plugging the explicit GS approximation (1.9) into $I_1(\mathbf{x})$ yields

$$I_1(\mathbf{x}) = \int_{\mathbb{R}^d} \sum_{q=0}^{S} w_q\, e^{-\tau_q^2 |\mathbf{y}|^2} \rho(\mathbf{x} - \mathbf{y}) d\mathbf{y}, \qquad \mathbf{x} \in \mathbf{B}_1 \tag{2.10}$$

$$= \sum_{q=0}^{S} w_q \int_{\mathbf{B}_{\mathbf{x},1}} e^{-\tau_q^2 |\mathbf{y}|^2} \rho(\mathbf{x} - \mathbf{y}) d\mathbf{y}, \qquad \mathbf{x} \in \mathbf{B}_1 \tag{2.11}$$

$$= \sum_{q=0}^{S} w_q \int_{\mathbf{B}_2} e^{-\tau_q^2 |\mathbf{y}|^2} \rho(\mathbf{x} - \mathbf{y}) d\mathbf{y}, \qquad \mathbf{x} \in \mathbf{B}_1, \tag{2.12}$$

where $\mathbf{B}_{\mathbf{x},1} := \mathbf{B}_1 + \mathbf{x}$ is the unit box centered at $\mathbf{x}$. Identity (2.12) holds because $\rho(\mathbf{x} - \mathbf{y}) = 0, \forall\, \mathbf{x} \in \mathbf{B}_1,\ \mathbf{y} \in \mathbf{B}_2 \setminus \mathbf{B}_{\mathbf{x},1}$. For $\mathbf{x} \in \mathbf{B}_1$ and $\mathbf{y} \in \mathbf{B}_2$ holds $\mathbf{x} - \mathbf{y} \in \mathbf{B}_3$, and we can approximate the density on $\mathbf{B}_3$ by a Fourier pseudo-spectral method with spectral accuracy [31]. More specifically, a simple zero-padding of the density from $\mathbf{B}_1$ to $\mathbf{B}_3$ is applied first, and the padded density ρ is well resolved by the following finite Fourier series:

$$\rho(\mathbf{z}) \approx \sum_{\mathbf{k}} \widehat{\rho}_{\mathbf{k}} \prod_{j=1}^{d} e^{\frac{2\pi i\, k_j}{b_j - a_j}(z^{(j)} - a_j)}, \qquad \mathbf{z} = (z^{(1)}, \ldots, z^{(d)}) \in \mathbf{B}_3, \tag{2.13}$$

where $a_j = -3, b_j = 3, j = 1, \ldots, d$ and $\mathbf{k} = (k_1, \ldots, k_d) \in \mathbb{Z}^d$ with $k_j = -\widetilde{n}_j/2, \ldots, \widetilde{n}_j/2 - 1$ and $\widetilde{n}_j = 3n_j$. The Fourier coefficients are determined as follows:

$$\widehat{\rho}_{\mathbf{k}} = \frac{1}{|\mathbf{B}_3|} \int_{\mathbf{B}_3} \rho(\mathbf{z}) \prod_{j=1}^{d} e^{\frac{-2\pi i\, k_j}{b_j - a_j}(z^{(j)} - a_j)} d\mathbf{z}, \tag{2.14}$$

where $|\mathbf{B}_3| = \prod_{j=1}^{d}(b_j - a_j)$ is the volume. The above integral is approximated by a trapezoidal rule, and the summation is accelerated by Fast Fourier Transform (FFT) [28].

Plugging (2.13) into (2.12), we have

$$I_1(\mathbf{x}) = \sum_{q=0}^{S} w_q \int_{\mathbf{B}_2} e^{-\tau_q^2 |\mathbf{y}|^2} \rho(\mathbf{x} - \mathbf{y}) d\mathbf{y} \tag{2.15}$$

$$\approx \sum_{q=0}^{S} w_q \sum_{\mathbf{k}} \widehat{\rho}_{\mathbf{k}} \prod_{j=1}^{d} e^{\frac{2\pi i\, k_j}{b_j - a_j}(x^{(j)} - a_j)} \int_{\mathbf{B}_2} e^{-\tau_q^2 |\mathbf{y}|^2} \prod_{j=1}^{d} e^{\frac{-2\pi i\, k_j\, y^{(j)}}{b_j - a_j}} d\mathbf{y} \tag{2.16}$$

$$= \sum_{q=0}^{S} w_q \sum_{\mathbf{k}} \widehat{\rho}_{\mathbf{k}} \prod_{j=1}^{d} e^{\frac{2\pi i\, k_j}{b_j - a_j}(x^{(j)} - a_j)} \prod_{j=1}^{d} \int_{-2}^{2} e^{-\tau_q^2 |y^{(j)}|^2} e^{\frac{-2\pi i\, k_j\, y^{(j)}}{b_j - a_j}} dy^{(j)} \tag{2.17}$$

$$= \sum_{\mathbf{k}} \widehat{\rho}_{\mathbf{k}} \left(\sum_{q=0}^{S} w_q G_{\mathbf{k}}^q \right) \prod_{j=1}^{d} e^{\frac{2\pi i\, k_j}{b_j - a_j}(x^{(j)} - a_j)}, \tag{2.18}$$

where

$$G_{\mathbf{k}}^q = \prod_{j=1}^{d} \int_{-2}^{2} e^{-\tau_q^2 |y^{(j)}|^2} e^{\frac{-2\pi i k_j\, y^{(j)}}{b_j - a_j}} dy^{(j)} = \prod_{j=1}^{d} \int_{0}^{2} 2\, e^{-\tau_q^2 |y^{(j)}|^2} \cos\left(\frac{2\pi k_j\, y^{(j)}}{b_j - a_j}\right) dy^{(j)}. \tag{2.19}$$

The coefficients in (2.19) are tensor products for any fixed index q. Notice that $G_{\mathbf{k}}^q$ does not depend on the mesh size $\vec{h} := (h^1, \ldots, h^d)^T$ or the density ρ. Therefore, it can be pre-computed, which greatly enhances
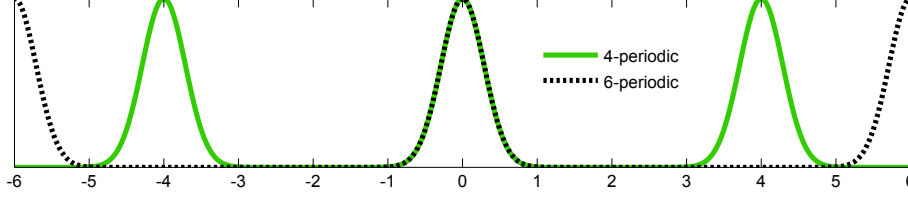
5

Figure 1: The 4-periodic (green-solid) and the 6-periodic (black-dotted) extension coincide on $\mathbf{B}_3$.

the efficiency of the evaluation of I_1, because the potential is usually solved many times in simulations. For a given discretization, we can pre-compute and store the sums of coefficients, i.e., $\sum_{q=0}^{S} w_q G_{\mathbf{k}}^q$, which helps to decrease the CPU-time dramatically at a small expense of storage. To compute $G_{\mathbf{k}}^q$, we only need to calculate three 1-dimensional vectors whose components are given as integrals. The integrals in (2.19) can be evaluated numerically by a Gauss-Kronrod quadrature up to machine precision [26]. Once $\sum_{q=0}^{S} w_q G_{\mathbf{k}}^q$ is known, $I_1(\mathbf{x})$ can be computed by (2.18) and the summation can be accelerated by FFT.

Remark 2.1. *Actually, we can restrict the zero-padding to $\boldsymbol{B}_2$ and apply the Fourier series approximation (2.13) on $\boldsymbol{B}_2$ instead of $\boldsymbol{B}_3$. This can be inferred from the fact that the 4-periodic and the 6-periodic extension of the density coincide on $\boldsymbol{B}_3$, see Fig. 1. Correspondingly, the constants in (2.13) will be changed to $a_j = -2, b_j = 2, \widetilde{n_j} = 2\, n_j, j = 1, \ldots, d$.*

2.2. Evaluation of the singular correction integral $I_2(\mathbf{x})$

For the purpose of evaluating $I_2(\mathbf{x})$, we first split it into two integrals as

$$
\begin{aligned}
I_2(\mathbf{x}) &= \int_{\mathbb{R}^d} (U(\mathbf{y}) - U_{GS}(\mathbf{y}))\, \rho(\mathbf{x} - \mathbf{y}) d\mathbf{y}, \quad \mathbf{x} \in \mathbf{B}_1 && (2.20) \\
&= \left(\int_{\mathcal{B}_\delta} + \int_{\mathbb{R}^d \setminus \mathcal{B}_\delta} \right) (U(\mathbf{y}) - U_{GS}(\mathbf{y}))\, \rho(\mathbf{x} - \mathbf{y}) d\mathbf{y}, \qquad \mathbf{x} \in \mathbf{B}_1 && (2.21) \\
&:= I_{2,1}(\mathbf{x}) + I_{2,2}(\mathbf{x}), \qquad \mathbf{x} \in \mathbf{B}_1. && (2.22)
\end{aligned}
$$

As can be inferred from the compactness assumption, i.e., $\mathrm{supp}(\rho) \subset \mathbf{B}_1$, we have for $\mathbf{x} \in \mathbf{B}_1$ that $\mathrm{supp}\{\rho(\mathbf{x} - \mathbf{y})\} \subset \mathbf{B}_2$. Therefore, the latter integral $I_{2,2}(\mathbf{x})$ is equivalent to an integral defined on a bounded domain, i.e., $\mathcal{D} := \mathbf{B}_2 \setminus \mathcal{B}_\delta$. To be more precise, we have

$$
\begin{aligned}
I_{2,2}(\mathbf{x}) &= \int_{\mathbb{R}^d \setminus \mathcal{B}_\delta} (U(\mathbf{y}) - U_{GS}(\mathbf{y}))\, \rho(\mathbf{x} - \mathbf{y}) d\mathbf{y}, \quad \mathbf{x} \in \mathbf{B}_1 && (2.23) \\
&= \int_{\mathcal{D}} (U(\mathbf{y}) - U_{GS}(\mathbf{y}))\, \rho(\mathbf{x} - \mathbf{y}) d\mathbf{y}, \qquad \mathbf{x} \in \mathbf{B}_1. && (2.24)
\end{aligned}
$$

Since the GS approximation of U gives an error ε on $\mathcal{D}$, we get the following estimate after introducing spherical/polar coordinates:

$$
|I_{2,2}(\mathbf{x})| \leq |S^{d-1}|\, \|\rho\|_\infty \int_\delta^2 r^{d-1}\, |U(r) - U_{GS}(r)|\, dr \leq C\, \|\rho\|_\infty \max_{r \in [\delta, 2]} |(U(r) - U_{GS}(r))|, \qquad (2.25)
$$

where $|S^{d-1}| = \frac{2\pi^{d/2}}{\Gamma(d/2)}$ is the volume of unit surface in $\mathbb{R}^d$ and C is a constant not depending on the density. We neglect $I_{2,2}$ because of the near-machine precision accurate GS approximation in (2.25).

6

Remark 2.2. *The error estimate in (2.25) does not really have to depend on the density ρ, simply because we can normalize the density at the very beginning, i.e. $\|\rho\|_\infty = 1$, see (1.6). In (2.25), the integral is actually over $r \in [\delta, 2\sqrt{d}]$. We neglected this issue for the sake of easier notation. In fact, it can be ultimately justified by rescaling the effective support into a smaller domain $\boldsymbol{B}_{1/\sqrt{d}}$.*

In order to compute $I_{2,1}$, we first need to interpolate the density function in a δ-neighborhood of $\mathbf{x}$. Since δ is small (we choose $\delta = 10^{-3}$ or 10^{-4} in our implementation), the interpolation of the density $\rho_{\mathbf{x}}(\mathbf{y}) := \rho(\mathbf{x} - \mathbf{y})$ within $\mathcal{B}_\delta$ can be done by the Taylor expansion. More precisely, we have

$$\rho_{\mathbf{x}}(\mathbf{y}) = P_{\mathbf{x}}(\mathbf{y}) + R_{\mathbf{x}}(\mathbf{y}), \quad \mathbf{y} \in \mathcal{B}_\delta, \tag{2.26}$$

where $P_{\mathbf{x}}(\mathbf{y})$, the third order Taylor expansion, is defined as follows:

$$P_{\mathbf{x}}(\mathbf{y}) = \rho_{\mathbf{x}}(\mathbf{0}) + \sum_{j=1}^d \frac{\partial \rho_{\mathbf{x}}(\mathbf{0})}{\partial y_j} y_j + \frac{1}{2} \sum_{j,k=1}^d \frac{\partial^2 \rho_{\mathbf{x}}(\mathbf{0})}{\partial y_j \partial y_k} y_j\, y_k + \frac{1}{6} \sum_{j,k,l=1}^d \frac{\partial^3 \rho_{\mathbf{x}}(\mathbf{0})}{\partial y_j \partial y_k \partial y_l} y_j\, y_k\, y_l, \tag{2.27}$$

and the remainder $R_{\mathbf{x}}(\mathbf{y}) = C(\rho, \mathbf{x})|\mathbf{y}|^4$ with the constant $C(\rho, \mathbf{x})$ depending on the density ρ and $\mathbf{x}$. Next, we plug the spherical/polar representation of (2.27) into (2.22), where we ignore the part $I_{2,2}$ as explained before. After integration over the variables $(r, \theta, \phi)/(r, \phi)$, the evaluation of $I_{2,1}$ comes down to simple multiplication of the Laplacian $\Delta \rho$ and some constants, since the contributions of the odd derivatives in (2.27) and off-diagonal components of the Hessian vanish. The derivatives of ρ are computed using the Fourier series approximation of ρ. It is worth mentioning that we do not have to resort to any numerical quadrature at this point. For example, to compute $\Delta \rho$, starting from (2.13) and differentiating the basis function, we have the following

$$\Delta \rho \approx \sum_{\mathbf{k}} \widehat{\rho}_{\mathbf{k}}\, \Delta \left(\prod_{j=1}^d e^{\frac{2\pi i\, k_j}{b_j - a_j}(z^{(j)} - a_j)} \right) \tag{2.28}$$

$$= \sum_{\mathbf{k}} \widehat{\rho}_{\mathbf{k}} \left[-\sum_{j=1}^d (\frac{2\pi\, k_j}{b_j - a_j})^2 \right] \prod_{j=1}^d e^{\frac{2\pi i\, k_j}{b_j - a_j}(z^{(j)} - a_j)}. \tag{2.29}$$

The approximation error of $I_{2,1}$ by $\widetilde{I_{2,1}}$ (the integral $I_{2,1}$ with Taylor expansion of ρ) is estimated as follows:

$$|(I_{2,1} - \widetilde{I_{2,1}})(\mathbf{x})| = \left| \int_{\mathcal{B}_\delta} (U(\mathbf{y}) - U_{GS}(\mathbf{y}))\, C(\rho, \mathbf{x})|\mathbf{y}|^4 d\mathbf{y} \right| \tag{2.30}$$

$$\leq \|C(\rho, \mathbf{x})\|_\infty |S^{d-1}| \left| \int_0^\delta r^{d-1}\, r^4 |U(r) - U_{GS}(r)| dr \right| \tag{2.31}$$

$$\leq \|C(\rho, \mathbf{x})\|_\infty\, |S^{d-1}|\, C_S \begin{cases} \delta^{d+3}, & \text{Coulomb kernel} \\ \delta^6\, |\log \delta|, & \text{Poisson kernel} \end{cases} \tag{2.32}$$

where

$$\widetilde{I_{2,1}}(\mathbf{x}) = \int_{\mathcal{B}_\delta} (U(\mathbf{y}) - U_{GS}(\mathbf{y}))\, P_{\mathbf{x}}(\mathbf{y}) d\mathbf{y}, \tag{2.33}$$

and C_S is a positive parameter depending on the weights of the GS approximation (see Sec. 3).

For the reader's convenience, we summarize the key steps of our method in Algorithm 1.

Remark 2.3. *The overall computational cost consists of two FFT evaluations of size $2^d N$ and two of size N plus $O(N)$ multiplications and additions, where $N = \prod_{j=1}^d n_j$ is the total number of grid points in the physical domain. The total memory storage is of size $O(N)$.*

7

Algorithm 1 Evaluation of the nonlocal potential (1.1)

Precomputation

1. Gaussian-sum approximation of the kernel $U(x)$ in (1.2).
2. Fourier coefficients $G_{\mathbf{k}}^q$ in (2.19) via its tensor product composing vectors.

Actual computation

1. Compute $\widehat{\rho}_{\mathbf{k}}$, see (2.14).
2. Evaluate I_1 by (2.18) with FFT.
3. Compute the Laplacian of ρ with FFT.
4. Evaluate $\widetilde{I_{2,1}}$ by (2.33).
5. Add I_1 and $\widetilde{I_{2,1}}$ to obtain the approximation of u.

2.3. Extension to the dipole-dipole potential

The dipole-dipole potential is of great importance in condensed matter and quantum mechanics [32, 33]. It also takes convolution form, i.e., $u(\mathbf{x}) = U * \rho$ where

$$
\begin{aligned}
U(\mathbf{x}) &= \frac{3}{4\pi} \frac{\mathbf{m} \cdot \mathbf{n} - 3(\mathbf{x} \cdot \mathbf{n})(\mathbf{m} \cdot \mathbf{x})/|\mathbf{x}|^2}{|\mathbf{x}|^3} & (2.34)\\
&= -(\mathbf{m} \cdot \mathbf{n})\delta(\mathbf{x}) - 3\,\partial_{\mathbf{nm}} \left(\frac{1}{4\pi|\mathbf{x}|} \right), \quad \mathbf{x} \in \mathbb{R}^3.
\end{aligned}
$$

Using the convolution theorem, we can rewrite the dipole-dipole potential as follows:

$$
u(\mathbf{x}) = -(\mathbf{m} \cdot \mathbf{n})\rho(\mathbf{x}) + \partial_{\mathbf{nm}} \left(\frac{1}{4\pi|\mathbf{x}|} \right) * \rho = -(\mathbf{m} \cdot \mathbf{n})\rho(\mathbf{x}) + \frac{1}{4\pi|\mathbf{x}|} * (\partial_{\mathbf{nm}}\rho). \tag{2.35}
$$

Therefore, the computation of u consists of the evaluation of the 3D Coulomb potential with the source term $\partial_{\mathbf{nm}}\rho(\mathbf{x})$. Since the density $\rho(\mathbf{x})$ is smooth and compactly supported in $\mathbf{B}_L$, it can be approximated by finite Fourier series with spectral accuracy, and so does the second derivative $\partial_{\mathbf{nm}}\rho(\mathbf{x})$. The source term $\partial_{\mathbf{nm}}\rho(\mathbf{x})$ can be easily computed with arithmetic operations of the discrete Fourier coefficients.

We note that a similar situation arises in the *Davey-Stewartson* nonlocal potential in 2D, where one could solve Poisson's equation with the second derivative of the density as source term. Hence, in the convolution form, one only has to convolve the 2D Poisson kernel with the second order derivative of the density, see example 5 in Sec. 4.

2.4. Anisotropic densities

For clarity, we assume that the (rescaled) density is compactly supported in the rectangular box $\mathbf{B}_{1,\eta} := [-1,1]^{d-1} \times \eta[-1,1]$. Here, the regular integral and correction integral need modifications accordingly. More precisely, for the evaluation of the regular integral, the related changes are listed as follows:

$$
I_1(\mathbf{x}) = \sum_{\mathbf{k}} \widehat{\rho}_{\mathbf{k}} \left(\sum_{q=0}^{S} w_q G_{\mathbf{k}}^q \right) e^{\frac{2\pi i}{\varepsilon(b_d - a_d)} k_d (x^{(d)} - \varepsilon a_d)} \prod_{j=1}^{d-1} e^{\frac{2\pi i}{b_j - a_j} k_j (x^{(j)} - a_j)}, \tag{2.36}
$$

where

$$
G_{\mathbf{k}}^q = \int_{-2\eta}^{2\eta} e^{-\tau_q^2 |y^{(d)}|^2} e^{\frac{-2\pi i k_d\, y^{(d)}}{\eta(b_d - a_d)}}\, dy^{(d)} \prod_{j=1}^{d-1} \int_{-2}^{2} e^{-\tau_q^2 |y^{(j)}|^2} e^{\frac{-2\pi i k_j\, y^{(j)}}{b_j - a_j}}\, dy^{(j)}. \tag{2.37}
$$

For the correction integral I_2, we have to choose $\delta < \eta$ so as to guarantee the validity and accuracy of the Taylor expansion. Numerical results for the 2D/3D Coulomb potentials are displayed in Section 4, see Tab. 5 and Tab. 3.

Remark 2.4. *Given a general rectangular domain, e.g., $[-L_x, L_x] \times [-L_y, L_y]$ in 2D, the above algorithm for anisotropic densities can then be adapted simply by setting $\eta = \min\{L_x/L_y, L_y/L_x\}$. The method for the 3D Coulomb potential evaluated on a more general rectangular domain can be adapted accordingly.*

3. Kernel approximation

The highly accurate approximation of the kernel in $[\delta, 2]$, $\delta > 0$ is of particular importance in our algorithm. Here we choose the GS approximation, which has already been exploited extensively in [9, 10, 11, 29]. Its tensor product structure leads to a considerable simplification of the pre-computation (2.19) in the evaluation of the regular integral I_1. The high accuracy in the GS approximation of the kernel in an interval $[\delta, 2]$ allows us to neglect the integral $I_{2,2}$, see (2.25). Consequently, the correction integral I_2 can be confined to a small ball $\mathcal{B}_\delta$.

We use the sinc quadrature approach to obtain the GS approximation, which relies on a Gaussian integral representation of the kernel U. In this section, we briefly review some facts of the *sinc quadrature* [22, 29] to make our paper reasonably self-contained, then present the concrete approximations of the kernels $1/r$ and $\ln r$ on an interval $[\delta, 2]$, $0 < \delta \ll 1$.

3.1. Sinc quadrature

The sinc function $\mathrm{sinc}(t) := \frac{\sin(\pi t)}{\pi t}$ is an analytic function, which equals to 1 at $t = 0$ and zero at $t \in \mathbb{Z} \setminus \{0\}$. Sufficiently fast decaying continuous functions $f \in C(\mathbb{R})$ can be interpolated at the grid points $t_k = k\vartheta \in \vartheta\mathbb{Z}$, $\vartheta > 0$ (step size) by functions $\mathcal{S}_{k,\vartheta}(t) := \mathrm{sinc}(t/\vartheta - k)$, i.e.,

$$f_\vartheta(t) = \sum_{k \in \mathbb{Z}} f(k\vartheta)\mathcal{S}_{k,\vartheta}(t). \tag{3.38}$$

Since $\int_\mathbb{R} \mathrm{sinc}(t)\, dt = 1$, an interpolatory quadrature for $\int_\mathbb{R} f(t)\, dt$ is given as follows:

$$\int_\mathbb{R} f(t)\, dt \approx \vartheta \sum_{k \in \mathbb{Z}} f(k\vartheta), \tag{3.39}$$

which can be viewed as "infinite trapezoidal rule" quadrature. Finite truncation to the first $2S+1$ terms, i.e., $k = -S, \ldots, S$, of the infinite sum leads to the *sinc quadrature rule* with the error $\vartheta \sum_{|k|>S} f(k\vartheta)$ depending on the decay-rate of f. For functions $f(z)$ in the Hardy space $H^1(D_\lambda)$, $\lambda < \pi/2$, i.e., $f(z)$ is holomorphic in the strip $D_\lambda := \{z \in \mathbb{C} : |\Im z| \leq \lambda\}$ and

$$N(f, D_\lambda) := \int_{\partial D_\lambda} |f(z)|\, |dz| = \int_\mathbb{R} \left(|f(t + i\lambda)| + |f(t - i\lambda)| \right) \mathrm{d}\, t < \infty, \tag{3.40}$$

if $f(z)$ also satisfies the double exponential decay property on the real axis, we have the following exponential error estimate for sinc quadrature approximation, see [22] (Proposition 2.1).

Proposition 1 ([22]). *Let $f \in H^1(D_\lambda)$ with $\lambda < \pi/2$. If f satisfies the double exponential decay condition, i.e.,*

$$|f(t)| \leq C \exp(-be^{a|t|}) \quad \forall\, t \in \mathbb{R} \quad with \quad a, b, C > 0, \tag{3.41}$$

then the quadrature error for the special choice $\vartheta = \ln(\frac{2\pi aS}{b})/(aS)$ satisfies

$$\left| \int_\mathbb{R} f(t)\, dt - \vartheta \sum_{|k| \leq S} f(k\vartheta) \right| \leq C\, N(f, D_\lambda) \exp\left(\frac{-2\pi\lambda aS}{\ln(2\pi aS/b)} \right). \tag{3.42}$$

Remark 3.1. *In the case of an integral expression $\int_{\mathbb{R}} g(t) \, e^{xh(t)} \, dt$, the constants in (3.42) depend on the parameter x. For some fixed x, an accuracy of $\varepsilon > 0$ can be achieved with $S = \mathcal{O}(|\ln \varepsilon| \cdot \ln |\ln \varepsilon|)$. Moreover, in our computations, we use the simplified step-size $\vartheta = c_0 \ln(S)/S$, see (3.42), as in [22] with some positive constant c_0 (i.e., $c_0 = 2.1$ for the Coulomb kernel and $c_0 = 1$ for the Poisson kernel).*

In the following, we first represent the kernels $1/|\mathbf{x}|$ and $\ln |\mathbf{x}|$ in Gaussian integral forms and then apply the sinc quadrature to obtain GS approximations. These approximations are valid in an interval $[\delta, 2]$ and used to split the convolution (1.1), see (1.7).

3.2. Approximation of the Coulomb kernel $1/r$ over $[\delta, 2]$

Starting from the following identity

$$\int_0^\infty \tau^\alpha e^{-\rho \tau^2} \, d\tau = \Gamma(\tfrac{\alpha+1}{2}) \rho^{-\frac{\alpha+1}{2}}, \ \rho > 0, \, \alpha > -1, \tag{3.43}$$

for $\alpha = 0$ and $\rho = |\mathbf{x}|^2$, we get the following Gaussian integral representation for the Coulomb kernel

$$\frac{1}{|\mathbf{x}|} = \frac{2}{\sqrt{\pi}} \int_0^\infty e^{-|\mathbf{x}|^2 \tau^2} \, d\tau = \frac{2}{\sqrt{\pi}} \int_0^\infty \prod_{p=1}^d e^{-x^{(p)2} \tau^2} \, d\tau. \tag{3.44}$$

Note that, applying some numerical quadrature to the integral $\int_0^\infty e^{-\rho \tau^2} d\tau$ leads to a GS approximation

$$\frac{1}{|\mathbf{x}|} \approx \sum_q w_q \prod_{j=1}^d e^{-\tau_q^2 x^{(j)2}}. \tag{3.45}$$

Remark 3.2. *For kernels $1/|\mathbf{x}|^\beta$, $\beta > 0$, choosing $\alpha = \beta - 1$, formula (3.43) gives a Gaussian integral representation analogous to that of the Coulomb kernel. Substituting $\rho = |\mathbf{x}|^2$ and applying the numerical quadrature, we obtain a GS approximation.*

The numerical quadrature we choose here is the sinc quadrature, see Sec. 3.1, which is suited for integrals $\int_{\mathbb{R}} f(t) \, dt$ with $f \in C(\mathbb{R})$ decaying sufficiently fast. More precisely, by a change of variables in (3.44), i.e., $\tau = \sinh t := \frac{1}{2}(e^t - e^{-t})$, the updated integrand lies in a Hardy space with double exponential decay condition. Hence, Proposition 1 applies, i.e., the sinc quadrature converges exponentially with respect to the number of Gaussian terms. Moreover, the integrand is an even function, thus, we end up with only $S + 1$ terms.

A detailed analysis (similar to that in [15]) shows that the quadrature for $1/r, r = |\mathbf{x}|$ is acceptable for an interval $r \in [\delta, 2]$, $0 < \delta \ll 1$. The left picture of Fig. 2 shows the relative error E_{rel} of the GS approximation, where $E_{\text{rel}} := \| 1 - \sum_{q=0}^S w_q \, r \, e^{-\tau_q^2 r^2} \|_{L^\infty((\delta,2])}$. We could observe the exponential convergence in S.

3.3. Approximation of the Poisson kernel $\ln r$ over $[\delta, 2]$

In this subsection we present a GS approximation for the 2D Poisson kernel $\ln |\mathbf{x}| := \ln \sqrt{x^{(1)2} + x^{(2)2}}$. Setting $\alpha = 1$ in (3.43), we have

$$\frac{1}{x^{(1)2} + x^{(2)2}} = \int_0^\infty e^{-(x^{(1)2} + x^{(2)2})\tau} \, d\tau. \tag{3.46}$$

By applying a change of variables $\tau = \ln(1 + \exp(\sinh t))$, the integration domain in (3.46) is now the whole real axis and the integrand has double exponential decay. Thus, we can apply the sinc quadrature ($2S + 1$ terms in this case) to obtain a GS approximation of $|\mathbf{x}|^{-2}$ in $[1, R]$, $R > 1$, from which we can change to
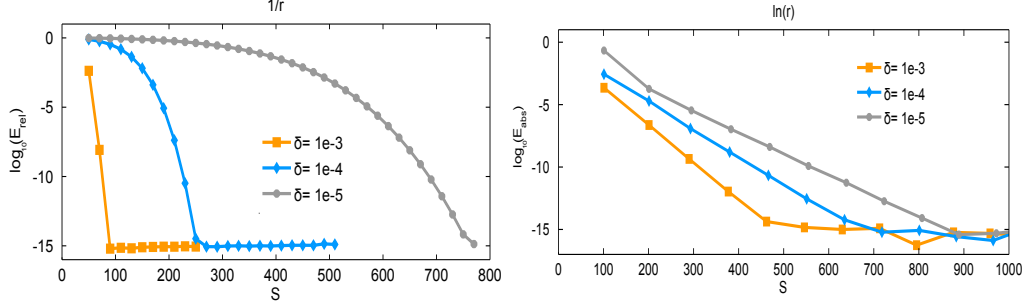
Figure 2: Number of terms S versus E_{rel} for the kernel $1/r$ (left), E_{abs} for $\ln r$ (right) on $[\delta, 2]$.

the interval $[\delta, 2]$ following a scaling argument. Inserting the GS approximation of $1/|\mathbf{x}|^2$ into the following formula

$$\ln \sqrt{x^{(1)^2} + x^{(2)^2}} = \int_{\sqrt{1-x^{(2)^2}}}^{x^{(1)}} \frac{y}{y^2 + x^{(2)^2}} \, dy, \tag{3.47}$$

we obtain an GS approximation of the Poisson kernel as follows:

$$\ln \sqrt{x^{(1)^2} + x^{(2)^2}} \approx C_0 - \sum_{q=1}^{S} \widetilde{w}_q \, e^{-\widetilde{\tau}_q (x^{(1)^2} + x^{(2)^2})} =: \sum_{q=0}^{S} w_q \, e^{-\tau_q^2 (x^{(1)^2} + x^{(2)^2})}, \tag{3.48}$$

where $w_0 = C_0$, $w_q = -\widetilde{w}_q$, $q \geq 1$ and $\tau_0 = 0$, $\tau_q = \widetilde{\tau}_q^{1/2}$, $q \geq 1$. Note that the coefficients w_q and τ_q in (3.48) should be computed stably (double precision) for both small and large nodes τ_q. The right figure in Fig. 2 shows the absolute error $E_{\text{abs}} := \| \ln r - \sum_{q=0}^{S} w_q \, e^{-\tau_q^2 r^2} \|_{L^\infty((\delta, 2])}$ for the kernel $\ln r$.

4. Numerical results

In order to demonstrate the accuracy and efficiency of our method, we perform several numerical tests in this section. All the numerical errors are calculated in the relative maximum norm, which is defined as follows

$$E := \frac{\|u - u_{\vec{h}}\|_{l^\infty}}{\|u\|_{l^\infty}} = \frac{\max_{\mathbf{x} \in \mathcal{T}_h} |u(\mathbf{x}) - u_{\vec{h}}(\mathbf{x})|}{\max_{\mathbf{x} \in \mathcal{T}_h} |u(\mathbf{x})|}, \tag{4.49}$$

where $\mathcal{T}_h$ is the rectangular computational domain discretized uniformly in each direction with mesh sizes $\vec{h} = (h_x, h_y)^T$ and $(h_x, h_y, h_z)^T$ for 2D and 3D, respectively. The grid function $u_{\vec{h}}$ is the numerical solution and u is the exact solution. Further, we denote the total number of grid points by $N := n_x n_y n_z$ and $N := n_x n_y$ for the 3D and 2D domain, respectively. For the sake of convenience, we denote the mesh sizes $\vec{h}$ simply by h if h_p is equal to each other.

The algorithm is implemented in FORTRAN, the code is compiled by ifort (version 14.0.2) using the option -O3, and executed on the Vienna Scientific Cluster (VSC-1). The CPU time shown in this section do not include the pre-computation time, since it is usually not relevant for most applications where the nonlocal potential is evaluated many times on the same grid.

Example 1. *The 3D Coulomb potential.*

11

For the density $\rho(\mathbf{x}) := e^{-(x^2+y^2+\gamma^2 z^2)/\sigma^2}$ with $\sigma > 0$ and $\gamma \geq 1$, the 3D Coulomb potential, with the kernel $U(\mathbf{x}) = \frac{1}{4\pi|\mathbf{x}|}$, can be computed analytically as

$$
u(\mathbf{x}) = \begin{cases} \frac{\sigma^3\sqrt{\pi}}{4\,|\mathbf{x}|}\operatorname{Erf}\left(\frac{|\mathbf{x}|}{\sigma}\right), & \gamma = 1, \\[2mm] \frac{\sigma^2}{4\gamma}\int_0^\infty \frac{e^{-\frac{x^2+y^2}{\sigma^2(t+1)}}\,e^{-\frac{z^2}{\sigma^2(t+\gamma^{-2})}}}{(t+1)\sqrt{t+\gamma^{-2}}}\,dt, & \gamma \neq 1, \end{cases} \quad \mathbf{x} \in \mathbb{R}^3, \tag{4.50}
$$

where $\operatorname{Erf}(x) = \frac{2}{\sqrt{\pi}}\int_0^x e^{-t^2}dt$ for $x \in \mathbb{R}$ is the error function. For densities $\rho_{\mathbf{x}_0}(\mathbf{x}) := \rho(\mathbf{x}-\mathbf{x}_0)$ with $\mathbf{x}_0 \in \mathbb{R}^3$, the corresponding 3D Coulomb potential is given exactly as $u_{\mathbf{x}_0}(\mathbf{x}) = u(\mathbf{x}-\mathbf{x}_0)$.

The 3D Coulomb potential is computed on $[-L,L]^2 \times [-L/\gamma, L/\gamma]$ with mesh size $h_x = h_y, h_z = h_x/\gamma$. Table 1 shows the errors E and computation time for the isotropic density, i.e., $\gamma = 1$, with $\sigma = 1.2$ on different domains $[-L,L]^3$, where T_1, T_2 and T_{total} denote hereafter the time for the evaluation of I_1, I_2 in (1.7) and the total time, respectively. Table 2 presents the results of the potential for shifted density with $\sigma = 1.2$ and $\mathbf{x}_0 = (1,2,1)^T$ computed on $[-12,12]^3$. Table 3 lists the errors E and timings for different anisotropic densities with $\sigma = 2$ computed on $[-12,12]^2 \times [-12/\gamma, 12/\gamma]$ using the same mesh size in x and y-direction, i.e., $h_x = h_y = 1/4$ and a different mesh size in z-direction, i.e., $h_z = h_x/\gamma$.

From Tab. 1-3, we can conclude that: (i) The method is spectral accurate with respect to the mesh size h and efficient with a complexity of $O(N \log N)$. (ii) The anisotropic potential can be computed with spectral accuracy without increasing the memory or CPU time as γ tends larger, thus, it is ideal for applications.

Table 1: Errors and timings of the 3D Coulomb potential in Example 1 with isotropic density with $\sigma = 1.2$ on $[-L,L]^3$.

$L = 8$	N	E	T_1	T_2	T_{total}
$h = 1$	16^3	1.096E-03	9.99E-04	1.00E-03	2.00E-03
$h = 1/2$	32^3	1.130E-09	1.60E-02	2.00E-03	1.80E-02
$h = 1/4$	64^3	6.169E-16	1.93E-01	1.90E-02	2.12E-01
$h = 1/8$	128^3	6.187E-16	1.69	6.28E-01	2.31
$h = 1/16$	256^3	7.725E-16	15.03	4.71	19.74
$L = 16$	N	E	T_1	T_2	T_{total}
$h = 1$	32^3	1.113E-03	1.60E-02	2.00E-03	1.80E-02
$h = 1/2$	64^3	1.191E-09	1.95E-01	2.10E-02	2.16E-01
$h = 1/4$	128^3	9.259E-16	1.71	6.22E-01	2.33
$h = 1/8$	256^3	9.271E-16	15.18	4.76	19.94

Table 2: Errors and timings of the 3D Coulomb potential in Example 1 for shifted Gaussian density with $\sigma = 1.2$ and $\mathbf{x}_0 = (1,2,1)^T$ on $[-12,12]^3$.

$L=12$	N	E	T_1	T_2	T_{total}
$h = 1$	24^3	1.108E-03	7.00E-03	4.00E-03	1.10E-02
$h=1/2$	48^3	1.175E-09	8.10E-02	1.20E-02	9.30E-02
$h=1/4$	96^3	6.182E-16	7.03E-01	1.08E-01	8.11E-01
$h=1/8$	192^3	7.717E-16	6.30	1.08	7.37

Example 2. *The 2D Coulomb potential.*

Table 3: Errors and timings of the 3D Coulomb potential in Example 1 for anisotropic densities with $\sigma = 2$ computed on $[-12, 12]^2 \times \frac{1}{\gamma}[-12, 12]$ with $h_x = h_y = 1/4, h_z = h_x/\gamma$ ($N = 96^3$).

γ	E	$\|u\|_{\max}$	T_1	T_2	T_{total}
1	4.486E-16	2	6.76E-01	1.01E-01	7.77E-01
2	5.599E-16	1.209	6.83E-01	1.02E-01	7.85E-01
4	1.427E-15	0.681	6.81E-01	1.00E-01	7.81E-01
8	2.606E-14	0.364	6.78E-01	1.03E-01	7.81E-01

For the density $\rho(\mathbf{x}) = e^{-(x^2+\gamma^2 y^2)/\sigma^2}$ with $\sigma > 0$ and $\gamma \geq 1$, the 2D Coulomb potential, with the kernel $U(\mathbf{x}) = \frac{1}{2\pi|\mathbf{x}|}$, can be obtained analytically as

$$u(\mathbf{x}) = \begin{cases} \frac{\sqrt{\pi}\,\sigma}{2}\,\mathrm{I}_0\left(\frac{|\mathbf{x}|^2}{2\sigma^2}\right) e^{-\frac{|\mathbf{x}|^2}{2\sigma^2}}, & \gamma = 1, \\ \frac{\sigma}{\gamma\sqrt{\pi}}\int_0^\infty \frac{e^{-\frac{x^2}{\sigma^2(t^2+1)}} e^{-\frac{y^2}{\sigma^2(t^2+\gamma^{-2})}}}{\sqrt{t^2+1}\sqrt{t^2+\gamma^{-2}}}\,dt, & \gamma \neq 1, \end{cases} \quad \mathbf{x} \in \mathbb{R}^2, \tag{4.51}$$

where I_0 is the modified Bessel function of the first kind [1].

Similarly, we shall first present the accuracy and efficiency of our method on fixed domains $[-L, L]^2$ with $\sigma = 1.2$ in Table 4. We compute the 2D Coulomb potential for anisotropic densities on $[-L, L] \times [-L/\gamma, L/\gamma]$ using a fixed mesh size in x-direction, i.e., $h_x = 1/4$, and different mesh sizes in y-direction, i.e., $h_y = h_x/\gamma$, see Table 5. From Tab.4 and Tab.5, we can draw similar conclusions as in the case of the 3D Coulomb potential.

Table 4: Errors and timings of the 2D Coulomb potential in Example 2 for $\sigma = 1.2$ on $[-L, L]^2$ with different mesh sizes.

$L = 8$	N	E	T_1	T_2	T_{total}
$h = 1$	16^2	9.426E-04	0	0	0
$h=1/2$	32^2	1.720E-09	0	0	0
$h=1/4$	64^2	4.190E-16	2.00E-03	1.01E-03	3.00E-03
$h=1/8$	128^2	5.229E-16	6.00E-03	2.00E-03	8.00E-03
$h=1/16$	256^2	5.229E-16	2.30E-02	7.01E-03	3.00E-02
$L = 16$	N	E	T_1	T_2	T_{total}
$h = 1$	32^2	9.576E-04	1.00E-03	0	1.00E-03
$h=1/2$	64^2	1.815E-09	1.00E-03	0	1.00E-03
$h=1/4$	128^2	5.846E-15	5.00E-03	2.00E-03	7.00E-03
$h=1/8$	256^2	5.846E-15	2.60E-02	7.00E-03	3.30E-02
$h=1/16$	512^2	6.055E-15	2.47E-01	2.80E-02	2.75E-01

Example 3. *The 2D Poisson potential.*

For $\rho(\mathbf{x}) := e^{-|\mathbf{x}|^2/\sigma^2} = e^{-r^2/\sigma^2}$ with $r = |\mathbf{x}|$ and $\sigma > 0$, the 2D Poisson potential, with the kernel $U(\mathbf{x}) = -\frac{1}{2\pi}\ln|\mathbf{x}|$, can be obtained analytically as

$$u(\mathbf{x}) = \begin{cases} -\frac{\sigma^2}{4}\left[\mathrm{E}_1\left(\frac{|\mathbf{x}|^2}{\sigma^2}\right) + 2\ln(|\mathbf{x}|)\right], & \mathbf{x} \neq \mathbf{0}, \\ \frac{\sigma^2}{4}\left(\gamma_e - \ln(\sigma^2)\right), & \mathbf{x} = \mathbf{0}, \end{cases} \tag{4.52}$$

13

Table 5: Errors and timings of the 2D Coulomb potential in Example 2 for anisotropic densities with $\sigma = 2$ computed on $[-12, 12] \times \frac{1}{\gamma}[-12, 12]$ with $h_x = 1/8, h_y = h_x/\gamma$ and $N = 192^2$.

γ	E	$\|u\|_{\max}$	T_1	T_2	T_{total}
1	5.047E-16	1.773	1.00E-02	2.00E-03	1.20E-02
2	5.479E-16	1.217	1.20E-02	3.00E-03	1.50E-02
4	4.235E-16	7.902E-01	9.00E-03	2.00E-03	1.10E-02
8	1.402E-15	4.902E-01	1.20E-02	2.00E-03	1.40E-02
16	8.387E-15	2.935E-01	1.20E-02	2.00E-03	1.40E-02

where $\mathrm{E}_1(r) := \int_r^\infty t^{-1} e^{-t} dt$ for $r > 0$ is the exponential integral function [1] and $\gamma_e \approx 0.5772156649015328606$ is the Euler-Mascheroni constant.

The 2D Poisson potential is computed on $[-L, L]^2$ with mesh size $h_x = h_y$. Table 6 shows the errors E and computation time with $\sigma = 1.2$ on $[-L, L]^2$ with different mesh sizes. Spectral accuracy and $O(N \log N)$ scaling can be observed from Tab. 6.

Table 6: Errors and timings of the 2D Poisson potential in Example 3 with $\sigma = 1.2$ on $[-L, L]^2$.

$L = 8$	N	E	T_1	T_2	T_{total}
$h = 1$	16^2	3.768E-04	0	0	0
$h=1/2$	32^2	3.331E-10	1.00E-03	0	1.00E-03
$h=1/4$	64^2	3.623E-15	2.00E-03	1.00E-03	3.00E-03
$h=1/8$	128^2	2.988E-15	6.00E-03	1.00E-03	7.00E-03
$h=1/16$	256^2	5.085E-15	2.30E-02	4.00E-03	2.70E-02
$L=16$	N	E	T_1	T_2	T_{total}
$h = 1$	32^2	2.966E-04	1.00E-04	0	1.00E-03
$h=1/2$	64^2	2.713E-10	2.00E-03	0	2.00E-03
$h=1/4$	128^2	3.856E-15	6.00E-03	2.00E-03	8.00E-03
$h=1/8$	256^2	3.164E-15	2.60E-02	6.00E-03	3.20E-02
$h=1/16$	512^2	6.921E-15	2.47E-01	3.00E-02	2.77E-01

Example 4. *The dipole-dipole potential in 3D.*

The 3D dipole-dipole potential is defined by convolution as follows [3, 4, 23]:

$$u(\mathbf{x}) \;=\; -(\mathbf{n} \cdot \mathbf{m}) \, \rho(\mathbf{x}) - 3 \, \partial_{\mathbf{nm}} \left(\frac{1}{4\pi|\mathbf{x}|} * \rho \right) = -(\mathbf{n} \cdot \mathbf{m}) \, \rho(\mathbf{x}) - 3 \, \frac{1}{4\pi|\mathbf{x}|} * (\partial_{\mathbf{nm}} \rho) \qquad (4.53)$$

where $\mathbf{n}, \mathbf{m}$ are two given unit vectors in $\mathbb{R}^3$. Note that the dipole-dipole potential can actually be calculated via the Coulomb potential by (4.53) with the new source term $(\partial_{\mathbf{nm}}\rho)$. Numerically, the source term $(\partial_{\mathbf{nm}}\rho)$ can be easily obtained by differentiating the Fourier pseudospectral approximation of ρ, compare with (2.28).

Similarly, we consider a radial symmetric density $\rho(\mathbf{x}) = e^{-|\mathbf{x}|^2/\sigma^2}$, and the potential is given explicitly as

$$
\begin{aligned}
u(\mathbf{x}) \;=\;& -(\mathbf{n} \cdot \mathbf{m}) \, \rho(\mathbf{x}) - 3 \, \partial_{\mathbf{nm}} \left(\frac{1}{4\pi|\mathbf{x}|} * \rho \right) = -(\mathbf{n} \cdot \mathbf{m}) \, \rho(\mathbf{x}) - 3 \, \partial_{\mathbf{nm}} \left(\frac{\sigma^2 \sqrt{\pi}}{4} \frac{\mathrm{Erf}(r/\sigma)}{r/\sigma} \right) \qquad (4.54) \\
\;=\;& -(\mathbf{n} \cdot \mathbf{m}) \, \rho(\mathbf{x}) - 3 \, \mathbf{n}^T \mathbf{D} \, \mathbf{m},
\end{aligned}
$$

14

where δ_{ij} is the Dirac delta function and the Hessian matrix $\mathbf{D}$ is given as follows

$$\mathbf{D}_{ij} = \delta_{ij}\left(\frac{\sigma^2}{2r^2}e^{-\frac{r^2}{\sigma^2}} - \frac{\sigma^3\sqrt{\pi}}{4r^3}\mathrm{Erf}\left(\frac{r}{\sigma}\right)\right) +$$

$$\mathbf{x}_i\mathbf{x}_j\left(-\frac{3\,\sigma^2}{2\,r^4}e^{-\frac{r^2}{\sigma^2}} - \frac{1}{r^2}e^{-\frac{r^2}{\sigma^2}} + \frac{3\,\sigma^3\sqrt{\pi}}{4\,r^5}\mathrm{Erf}\left(\frac{r}{\sigma}\right)\right), \qquad i,j = 1,2,3.$$

Table 7 shows the errors and timings of the 3D dipole-dipole potential evaluation with $\sigma = 1.2$ and two randomly chosen vectors $\mathbf{n} = (0.82778, 0.41505, -0.37751)^T$, $\mathbf{m} = (0.3118, 0.9378, -0.15214)^T$ on $[-8,8]^3$. Here, T_{pre} is the CPU time for computing the source term $\partial_{\mathbf{nm}}\rho$, T_1, T_2 and T_{total} are the same as those defined previously. We observe spectral accuracy and the timings show the expected scaling $O(N\log N)$.

Table 7: Errors and timings of the 3D dipole-dipole potential in Example 4 with $\sigma = 1.2$, $\mathbf{n} = (0.82778, 0.41505, -0.37751)^T$, $\mathbf{m} = (0.3118, 0.9378, -0.15214)^T$ on $[-8,8]^3$.

$L = 8$	N	E	T_{pre}	T_1	T_2	T_{total}
$h = 1$	16^3	1.380E-02	0	2.00E-03	0	2.00E-03
$h=1/2$	32^3	2.647E-07	2.00E-03	1.50E-02	2.00E-03	1.90E-02
$h=1/4$	64^3	1.430E-14	1.70E-02	2.00E-01	1.90E-02	2.35E-01
$h=1/8$	128^3	4.076E-14	1.96E-01	1.68	2.20E-01	2.10

Example 5. *The Davey-Stewartson (DS) nonlocal potential.*

In the DS equation, the nonlocal potential can be given by a convolution as follows:

$$u(\mathbf{x}) = -\frac{1}{2\pi}\ln|\mathbf{x}| * (\partial_{xx}\rho), \qquad \mathbf{x} \in \mathbb{R}^2. \tag{4.55}$$

For a Gaussian density $\rho(x,y) = \pi\,e^{-\pi^2(x^2+y^2)}$, the DS nonlocal potential is given explicitly, in polar coordinates, as

$$\Phi(r,\theta) = -\left(\frac{\pi}{2}\,e^{-\pi^2 r^2} + \cos(2\theta)\,e^{-\pi^2 r^2}(2\pi r^2)^{-1}(1 + \pi^2 r^2 - e^{\pi^2 r^2})\right). \tag{4.56}$$

Table 8 displays the errors and computational time for the computation of the DS nonlocal potential on $[-8,8]^2$. We observe the scaling $O(N\log N)$ and rapid decrease of the error as the mesh size gets smaller, although the best reached precision is above those of the previous 2D Poisson/Coulomb examples. In this context, note that the parameter σ is larger compared to the preceding test in Example 3, i.e. a finer resolution would be needed for the more localized density.

Table 8: Errors and timings of the DS nonlocal potential in Example 5 on $[-8,8]^2$.

$L = 8$	N	E	T_1	T_2	T_{total}
$h=1/2$	32^2	1.474	1.00E-03	0	1.00E-03
$h=1/4$	64^2	5.720E-03	2.00E-03	0	2.00E-03
$h=1/8$	128^2	3.974E-09	5.00E-03	2.00E-04	6.00E-03
$h=1/16$	256^2	4.536E-13	2.20E-02	7.00E-03	2.80E-02

15

5. Conclusions

Starting from the convolution formulation, we presented an efficient and accurate algorithm for the computation of several standard nonlocal (long-range) potentials induced by smooth and fast decaying densities. The method uses a Gaussian-sum (GS) approximation of the singular convolution kernel in order to split the convolution into two integrals, namely a long-range regular and a short-range singular integral. The regular integral is computed with a Fourier method using FFT, while the singular integral evaluation makes use of a low-order Taylor expansion of the density and is realized via FFT as well. The algorithm achieves spectral accuracy and is essentially as efficient as the FFT algorithm with a computational complexity of $O(N \log N)$, where N is the total number of points in the discretization of physical space. The method was implemented in FORTRAN and verified for several different potentials, including the 2D/3D Coulomb potential, the 2D Poisson, the 3D dipole-dipole potential and the Davey-Stewartson nonlocal potential.

Acknowledgments

References

[1] M. Abbamowitz and I. Stegun, Handbook of Mathematical Functions, Dover, 1965.

[2] X. Antoine, Q. Tang and Y. Zhang, On the ground states and dynamics of space fractional nonlinear Schrödinger/Gross-Pitaevskii equations with rotation term and nonlocal nonlinear interactions, J. Comput. Phys. 325 (2016) 74–97.

[3] W. Bao and Y. Cai, Mathematical theory and numerical methods for Bose-Einstein condensation, Kinet. Relat. Mod. 6 (2013) 1–135.

[4] W. Bao, Y. Cai and H. Wang, Efficient numerical methods for computing ground states and dynamics of dipolar Bose-Einstein condensates, J. Comput. Phys. 229 (2010) 7874–7892.

[5] W. Bao, H. Jian, N. Mauser and Y. Zhang, Dimension reduction of the Schrödinger equation with Coulomb and anisotropic confining potentials, SIAM J. Appl. Math. 73 (6) (2013) 2100–2123.

[6] W. Bao, S. Jiang, Q. Tang and Y. Zhang, Computing the ground state and dynamics of the nonlinear Schrödinger equation with nonlocal interactions via the nonuniform FFT, J. Comput. Phys. 296 (2015) 72–89.

[7] W. Bao, Q. Tang and Y. Zhang, Accurate and efficient numerical methods for computing ground states and dynamics of dipolar Bose-Einstein condensates via the nonuniform FFT, Commun. Comput. Phys. 19(5) (2016) 1141–1166.

[8] G. Beylkin, C. Kurzc and L. Monzón, Fast convolution with the free space Helmholtz Green's function, J. Comput. Phys. 228 (2009) 2770-2791.

[9] G. Beylkin and L. Monzón, Approximation by exponential sums, Appl. Comput. Harmon. Anal. 19 (2005) 17-48.

[10] G. Beylkin and L. Monzón, Approximation by exponential sums revisited, Appl. Comput. Harmon. Anal. 28 (2010) 131-149.

[11] D. Braess and W. Hackbusch, On the efficient computation of high-dimensional integrals and the approximation by exponential sums, Multiscale, Nonlinear and Adaptive Approximations, Springer, 2009.

[12] A. Cerioni, L. Genovese, A. Mirone and V. Sole, Efficient and accurate solver of the three-dimensional screened and unscreened Poisson's equation with generic boundary conditions, J. Chem. Phys. 137 (2012) 134108.

[13] A. Dutt and V. Rokhlin, Fast Fourier transforms for nonequispaced data, SIAM J. Sci. Comput. 14 (1993) 1368–1393.

[14] F. Ethridge and L. Greengard, A new fast-multipole accelerated Poisson solver in two dimensions, SIAM J. Sci. Comput. 23 (3) (2001) 741–760.

[15] L. Exl, C. Abert, N. Mauser, T. Schrefl, H. Stimming and D. Suess, FFT-based Kronecker product approximation to micromagnetic long-range interactions, Math. Model Methods Appl. Sci. 24 (2014) 1877–1901.

[16] L. Exl, W. Auzinger, S. Bance, M. Gusenbauer, F. Reichel and T. Schrefl, Fast stray field computation on tensor grids, J. Comput. Phys. 231 (2012) 2840–2850.

[17] L. Exl and T. Schrefl, Non-uniform FFT for the finite element computation of the micromagnetic scalar potential, J. Comput. Phys. 270 (2014) 490-505.

[18] L. Füsti-Molnar and P. Pulay, Accurate molecular integrals and energies using combined plane wave and Gaussian basis sets in molecular electronic structure theory, J. Chem. Phys. 116 (2002) 7795.

[19] L. Genovese, T. Deutsch, A. Neelov, S. Goedecker and G. Beylkin, Efficient solution of Poisson equation with free boundary conditions, J. Chem. Phys. 125 (2006) 074105.

[20] L. Genovese, T. Deutsch and S. Goedecker, Efficient and accurate three-dimensional Poisson solver for surface problems, J. Chem. Phys. 127 (2007) 054704.

[21] L. Greengard and V. Rokhlin, A new version of the fast multipole method for the Laplace equation in three dimensions, Acta Numerica 6 (1997) 229–269.

[22] W. Hackbusch and B. Khoromskij, Low-rank Kronecker-product approximation to multi-dimensional nonlocal operators. Part I. Separable approximation of multi-variate functions, Computing 76 (3) (2006) 177–202.

[23] S. Jiang, L. Greengard and W. Bao, Fast and accurate evaluation of nonlocal Coulomb and dipole-dipole interactions via the nonuniform FFT, SIAM J. Sci. Comput. 36 (2014) B777–B794.

[24] G. Martyna and M. Tuckerman, A reciprocal space based method for treating long range interactions in ab initio and force-field-based calculations in clusters, J. Chem. Phys. 110 (1999) 2810–2821.

[25] N. Mauser and Y. Zhang, Exact artificial boundary condition for the Poisson equation in the simulation of the 2D Schrödinger-Poisson system, Commun. Comput. Phys. 16 (3) (2014) 764–780.

[26] R. Piessens, E. Doncker-Kapenga and C. Überhuber, QUADPACK: a subroutine package for automatic integration, Springer,1987.

[27] M. Pippig, PFFT: An extension of FFTW to massively parallel architectures, SIAM J. Sci. Comput. 35 (2013) C213–C236.

[28] J. Shen and T. Tang, Spectral and High-Order Methods with Applications, Science Press, Beijing, 2006.

[29] F. Stenger, Numerical Methods Based on Sinc and Analytic Functions, Springer-Verlag, 1993.

[30] H. Stimming, N. Mauser and Y. Zhang, A novel nonlocal potential solver based on nonuniform FFT for efficient simulation of the Davey-Stewartson equations, arXiv:1409.2014.

[31] L. Trefethen, Spectral Methods in Matlab,Oxford University, Oxford, 2000.

[32] S. Yi and L. You, Trapped atomic condensates with anisotropic interactions, Phys. Rev. A 61 (2000) 041604(R).

[33] S. Yi and L. You, Trapped condensates of atoms with dipole interactions, Phys. Rev. A 63 (2001) 053607.

[34] Y. Zhang and X. Dong, On the computation of ground states and dynamics of Schrödinger-Poisson-Slater system, J. Comput. Phys. 230 (2011) 2660–2676.